Invited Paper

Near-field measurements of the terahertz superconducting spectrometer for atmospheric observation

Jie Hu [1*, 2, 3], Sheng Li [1, 2], Chuan Su [1, 2, 3], Dong Liu [1, 2], Qi-Jun Yao [1, 2], Xiao-ling Zhang [1, 2, 4], Zheng Lou [1, 2], and Sheng-Cai Shi [1, 2]

[1] Purple Mountain Observatory, CAS, 2nd West Beijing Road, Nanjing, China

[2] Key Lab of Radio Astronomy, CAS, China.

[3] University of Chinese Academy of Science.

[4] University of Science and Technology of China.

[*] Email: jiehu@pmo.ac.cn

(Received December 10, 2017)

Abstract: The optical verification of a terahertz superconducting spectrometer (TSR) featured with superconducting-insulator-superconducting (SIS) receivers developed at Purple Mountain Observatory (PMO) for atmospheric profiling synthetic observation system project (APSOS) has been presented. Near-fields of TSR at 230 *GHz* and 280 *GHz* have been measured and far-fields are derived. The misalignment of the optics at 280 *GHz* is analysed in detail by physical optics (PO).

Keywords: Superconducting receiver, Near-field, Physical optics, SIS

doi: 10.11906/TST.034-042.2018.06.04

1. Introduction

APSOS is a ground-based atmospheric profiling observation system capable of measuring range-resolved parameters of the whole atmosphere, from surface to up 110 *km* with high vertical and temporal resolutions [1]. As a part of APSOS project, TSR [2, 3] is developed to monitor the vertical profiles of mesospheric water vapor and greenhouse gas over Yangbajing, Tibet. TSR is a dual-band terahertz receiver equipped with SIS mixers operating at 180~300 *GHz* and 300~400 *GHz* observing H_2O, O_3, ClO, HCN, et al in the zenith direction, making it important to well characterize the radiation patterns for successful operation of the system. The geometry of TSR antenna is a classical off-axis Cassegrain telescope with a diameter of 30 *cm* [4]. The front-end optics consists of a paraboloid mirror, a hyperbolic mirror and several plane mirror.

There are three ways to measure the radiation pattern of antenna at THz bands. The most straight-forward method is to place a probe in the far-field of the antenna and measure the radiation pattern by rotating the antenna under test (AUT), which requires the probe to be placed at least $2D^2/l$ away from the DUT [5], where D is the diameter of the antenna and l is the working wavelength. Another way to measure the radiation pattern is the compact antenna test range (CTAR) method [6]. The AUT is tested in the quite zone, where the spherical wave front of the feed is collimated to a plane wave front by reflectors, lens et al. The third method is to measure the near-field of the AUT. The far-field pattern is calculated from the measured data mathematically [7, 8].

The near-field measurements have been chosen to characterize the radiation pattern of TSR for two reasons. On the one hand, the far-field range required by TSR antenna is about 200 *m*. On the other hand, PMO has been developing planar near-field antenna measurement method since 2014 [9, 10], making the near-field measurement financially and temporal efficient.

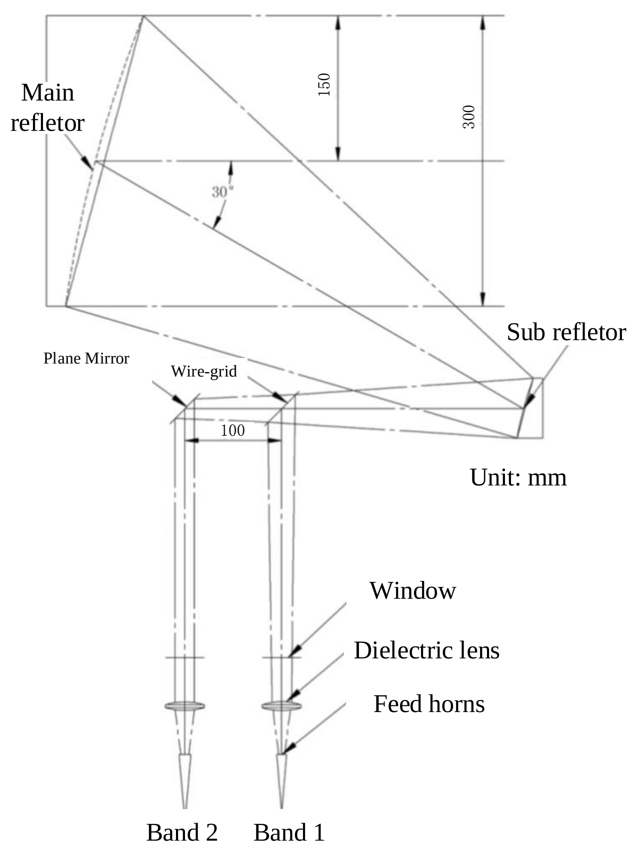

Fig. 1 Optical layout of TSR

In this paper, the near-field measurement of TSR telescope will be introduced and the result is compared with that of PO simulation. In section 2, the optical design of TSR will be introduced. In section 3, the near-field measurement setup will be presented. In part 4, measurement results at 230 *GHz* and 280 *GHz* will be shown. The measurement uncertainty will be given and the result at 280 *GHz* will be compared with PO simulation.

2. Design of TSR optics

TSR is a dual-band receiver with SIS as mixers and the optical layout of TSR shown in Fig. 1

[4]. The main optics of TSR is an off-axis Cassegrain telescope. The diameter of the main paraboloid mirror is 30 *cm* and its focal length is 1,200 *mm*. The sub-reflector is a hyperbolic mirror with the diameter of 64 *mm* and eccentricity of 1.6667. The bands of TSR are divided into band 1 (180~300 *GHz*) and band 2 (300~400 *GHz*) by a wire-grid. Band 1 and band 2 are separated by 100 *mm*. Band 1 is divided into two sub-bands, B1L (180~240 *GHz*) and B2L (240~300 *GHz*). The optical paths between the reflectors and window of the cryostat are modulated by a group of path length modulation (PLM) mirrors which consists of two roof mirrors. The lens are placed 50 *mm* away from the window of the cryostat. The design parameters of lens and corrugated horns are shown in Table. 1, which are determined to ensure the edge taper of the sub-reflector to be 13 *dB* for each band.

Tab. 1 Design parameters of lens and corrugated horns

Bands (*THz*)	Corrugated horn		Dielectric lens		
	Aperture Radius (*mm*)	Slant length (*mm*)	Radius of Curvature (*mm*)	Diameter (*mm*)	Thickness (*mm*)
180~240	5.60	54.32	87	40	7.66
240~300	6.00	55.07	83.2	40	7.88
300~	5.00	50.00	75.7	40	8.38

3. Measurement setup

The nearfield measurement setup is shown in Fig. 2. The detectors used are SIS mixers working in two different bands and the measured receiver noise temperature of the system is well below 250 *K* [11]. The RF and LO signals are both generated by microwave synthesizers followed by amplifier-multiplier-chains (AMC) with multiplication factor of 18. The LO signal is injected into SIS mixer by horn-to-horn power transmission system to achieve both high power efficiency and good thermal isolation. The intermediate frequency (IF) is set to be 360 *MHz* and the reference frequency is 20 *MHz*. The IF and the reference signal are acquired by a high speed ADC with 800 *MHz/s* sample rate.

The probe used is a wr-3.4 open-end waveguide, thus no probe compensation is applied as the effect of the probe is negligible and it is aligned with TSR by laser. The probe is placed about 1,000 *mm* away from the main paraboloid mirror on a XY scanner with positioning accuracy about 15 μm. The range of the scanner is 288 *mm* in each axis, which is a bit smaller than the diameter of the main paraboloid. There will be phase error introduced by the flexible cable connecting to the RF AMC as it will move with the scanner during the nearfield scan. The phase error introduced by the flexible cable is not calibrated due to the limited bandwidth of the circulator used in our system [10] and its effect will be discussed later.

The nearfield of TSR is scanned by on-the-fly (OTF) scan method [10] at the speed of 30 *mm/s* along X direction shown in Fig. 2 (b) and the step in Y direction is 3 *mm*. The scanned area is 288×288 *mm*. Calibration is done by moving the probe to the center of the scan area every three scanning lines and it takes about 2,000 *s* to finish a nearfield scan.

Nearfield measurements of TSR at B1L (230 *GHz*) and B2 (280 *GHz*) has been carried out. The measurement frequency of B2 is chosen at 280 *GHz* as the working frequency of the reference mixer is limited to 16 *GHz*.

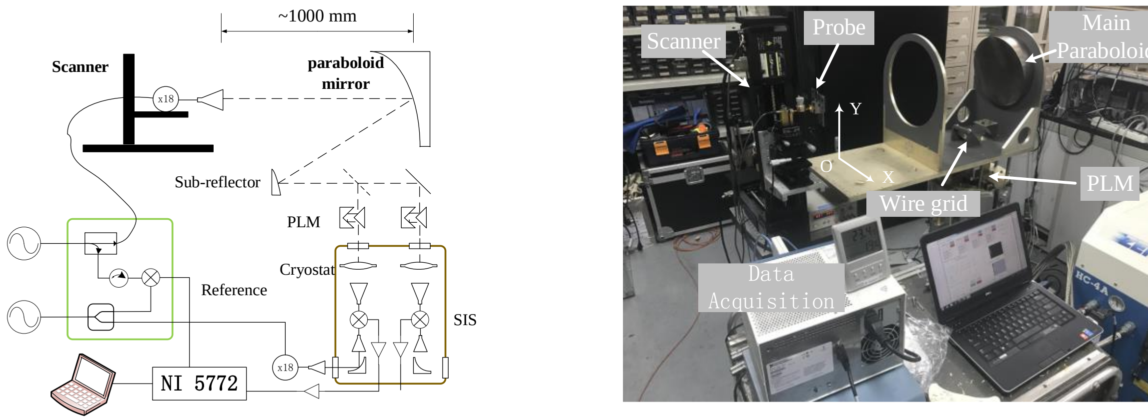

(a) (b)

Fig. 2 Setup of TSR nearfield measurement: (a) Nearfield measurement scheme (b) Photo of nearfield measurement

4. Results and analysis

The measured nearfields of TSR at B1 (230 *GHz*) and B2 (280 *GHz*) are shown in Fig. 3 and Fig. 4. There are obvious truncation of the nearfield due to the limited scan area in both bands. The measured amplitude at the edge of the scan area is about -20 *dB* relative to the maximum. The scanning effect has been calibrated and the data sampled along the X direction are interpreted to 3 *mm* spacing, the same with that along with the Y direction.

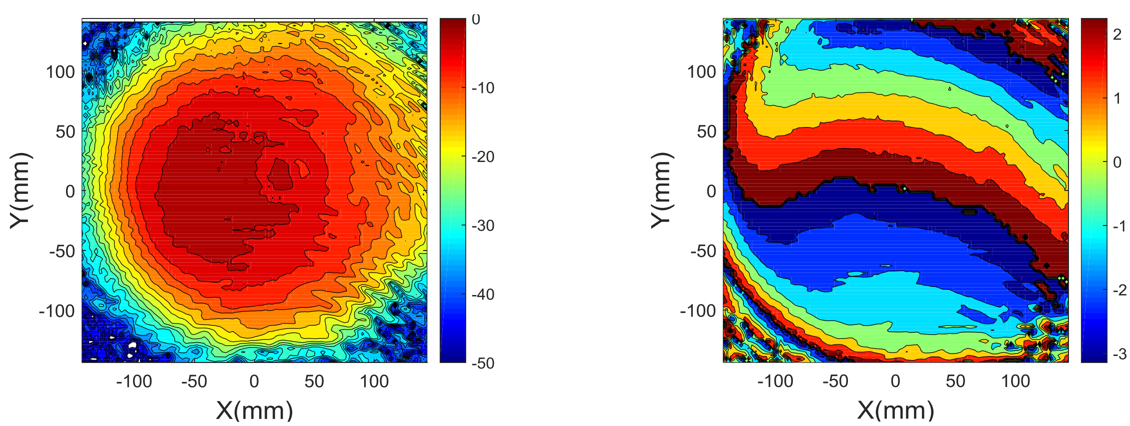

(a) (b)

Fig. 3 Measured nearfield amplitude and phase of B1L at 230 *GHz*: (a) amplitude (dB) (b) phase (rad)

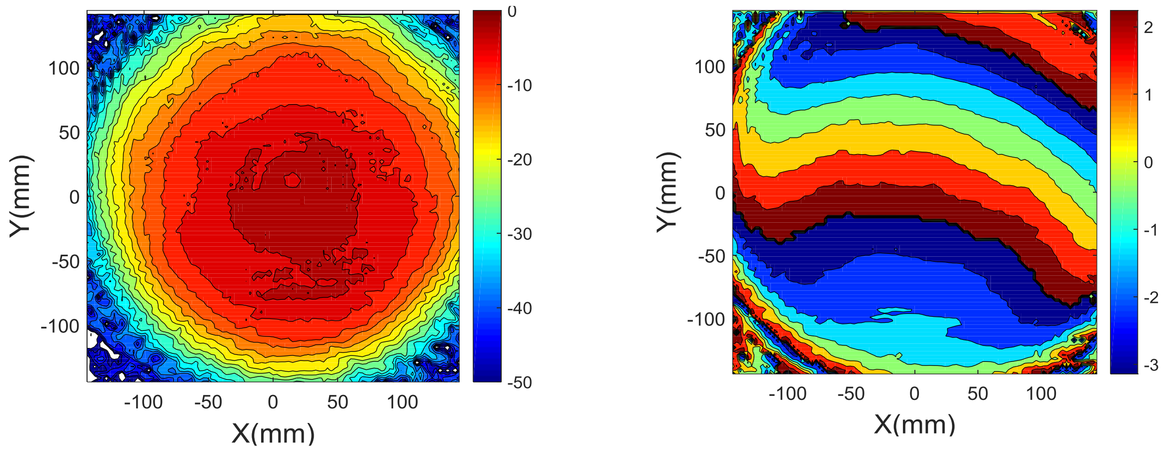

(a) (b)

Fig. 4 Measured nearfield amplitude and phase of B2 at 280 *GHz*: (a) amplitude (dB) (b) phase (rad)

The farfields calculated from the near-field is shown in Fig. 5, which shows good symmetry in both B1 and B2 band. The measured HPBW of B1 and B2 are 0.32 *deg* and 0.28 *deg* at 230 *GHz* and 280 *GHz* respectively. The measured first sidelode level of B1 and B2 at 230 *GHz* are about -17 *dB* and -27 *dB*. The main beam of TSR is steered off the main optic axis duo to the misalignment of the optic components. The beam offsets of B1 is 0.08 *deg* in azimuth and 0.38 *deg* in elevation at 230 *GHz*. And the beam offset of B2 at 280 *GHz* is 0.08 *deg* in azimuth and 0.34 *deg* in elevation. The main farfield parameters of B1 and B2 are compared in Table 2.

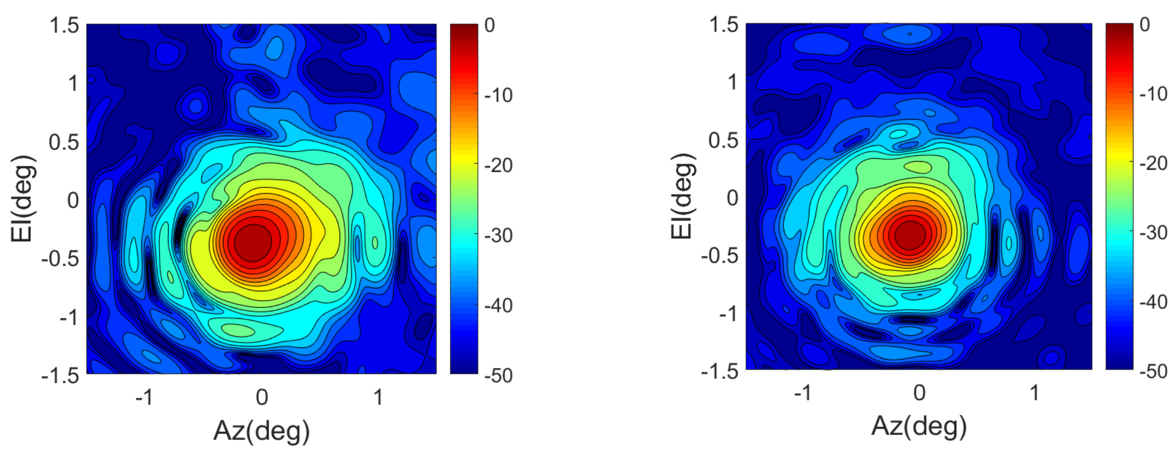

(a) (b)

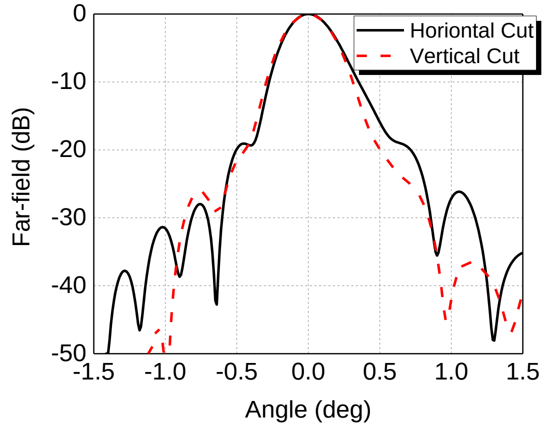

(c)

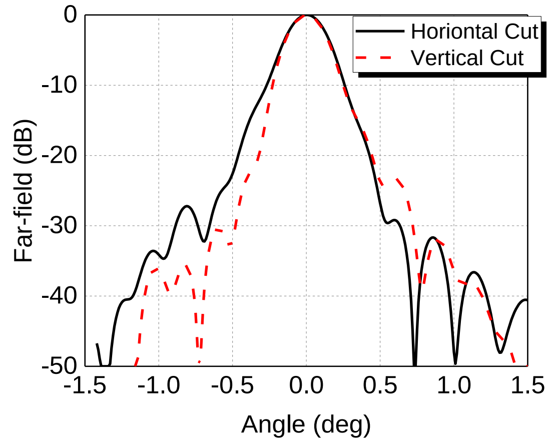

(d)

Fig. 5 Derived far-fields amplitude of TSR: (a) 2D farfield of TSR at 230 *GHz* (Unit: dB) (b) 2D farfield of TSR at 280 *GHz* (Unit: dB) (c) 1D farfield through the center at 230 *GHz* (d) 1D farfield through the center at 280 *GHz*.

Tab. 2 Main farfield beam parameters of B1 and B2

	HPBW(*deg*)	Sidelobe Level (*dB*)	Offset in El (*deg*)	Offset in Az(*deg*)
B1 (230 *GHz*)	0.32	-17	0.38	0.08
B2 (280 *GHz*)	0.28	-27	0.34	0.08

The main measurement errors in our system at -30 *dB* sidelobe are the truncation error, the planarity of the scanning plane, the long term drift during the measurement and the phase error introduced by the flexible cable connecting the AMC on the XY scanner which are listed in Table 3. The error budget is obtained by comparing the resulting farfield of the unprocessed and the processed nearfield data or by comparison with simulation where measurements were not available. The truncation error is relatively large compared with other nearfield measurement system because of the limited scanning range which is smaller than the size of the main paraboloid. The phase error of the flexible cable is obtained after the nearfield scan.

Tab. 3 Main Error Budget at -30 *dB* sidelobe of the nearfield scan of TSR (Unit: dB)

	B1L (230 *GHz*)	B2 (280 *GHz*)	Analysis technique	Note
Truncation	0.3	2.4	Simulation	Comparing simulation data with and without truncation
Planarity of the scanning plane	3.8	4.1	Theoretical Calculation	Theoretical calculation from eq. from [12]
Long term drift	4.2	6.0	Simulation	Comparing unprocessed and processed farfield data
Flexible cable	3.8	4.5	Simulation	Comparing measured data with and without cable phase error

The optical misalignments of B2 have been carefully studied by comparing the transformed and the simulated farfields by home-made physical optics (PO) software, EPOR [13]. The cost function is defined as [8]

$$C = \sum (|E_{0x} - E_{0t}|) + \sum |E_{90x} - E_{90t}|$$

where E_{0x} and E_{90x} is amplitude of the transformed farfields from measurement and E_{0t} and E_{90t} is the farfields from PO simulation. The simulated result of B2 at 280 *GHz* is shown in Fig. 6, which shows much better match with the measured result. The derived farfields from simulation is shown in Fig. 7. The most sensitive parameter of amplitude in our system is the lens displacement relative to the main optical axis while that of phase is the relative angle between the main paraboloid and the sub-reflector.

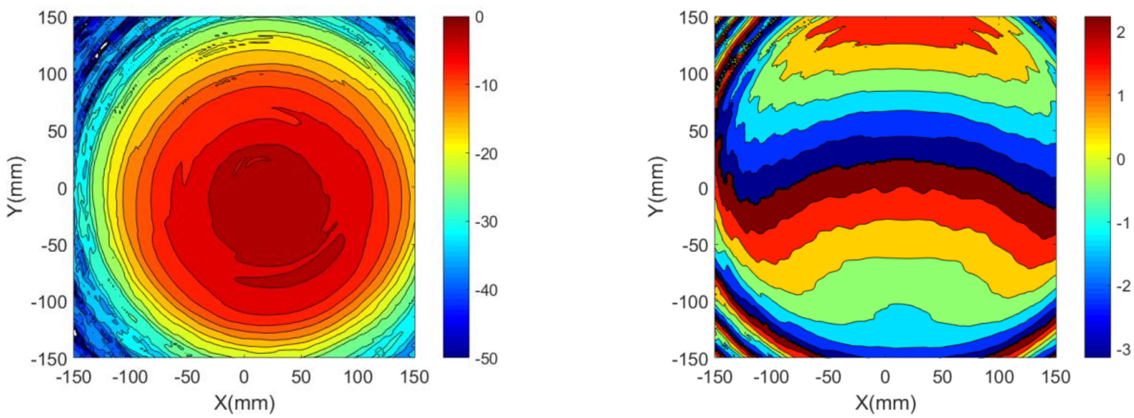

(a) (b)

Fig. 6 Simulated nearfield of B2 at 280 *GHz* with misalignment: (a) amplitude (Unit: dB) (b) phase (Unit: deg)

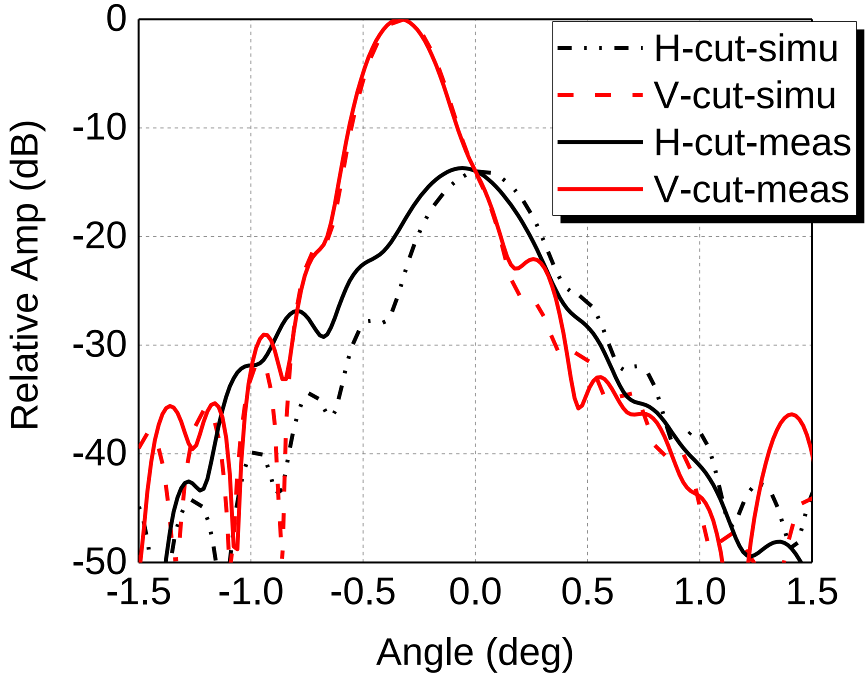

Fig. 7 Comparison between the measured and simulated farfield after taking optical misalignments into consideration

5. Conclusions

The radiation properties of the TSR telescope have been well characterized by planar near-field measurements for B1 at 230 *GHz* and for B2 at 280 *GHz*. The measured HPBW of B1 and B2 are 0.32 *deg* and 0.28 *deg* at 230 *GHz* and 280 *GHz* respectively. The first sidelobe of B1 at 230 *GHz* is -17 *dB* and that of B2 at 280 *GHz* is -27 *dB*. The PO simulation has been successfully carried out to simulate the misalignment of optics, which shows the most sensitive parameter of amplitude in our system is the lens displacement relative to the main optical axis while that of phase is the relative angle between the main paraboloid and the sub-reflector.

6. Acknowledgement

This work was supported in part by the National Natural Science Foundation of China (NSFC) under Grant No. 41127901, and by Chinese Academy of Sciences (CAS) project of QYZDJ-SSW-SLH043.

References

[1] D. Lu and W Pan. “Atmospheric profiling synthetic observation system (APSOS)”. *AIP Conference Proceedings*,

1531,244 (2013).

[2] Q. J. Yao, D. Liu, J. Li et al. “Atmospheric profiling synthetic observation system at THz”. *Proc. SPIE*, 8562, 314-318 (2012).

[3] Q. J. Yao, D. Liu, Z. Lin et al. “Atmospheric profiling synthetic observation system at THz wave band”. *2015 40th IRMMW-THz*, 1-2 (2015).

[4] D. Liu. “Optical design of terahertz superconducting spectrometer”. *Internal Report* (2014).

[5] A. Balanis. “Antenna theory: analysis and design”. *John Wiley & Sons* (2005).

[6] A. Lonnqvist. “Application of hologram-based compact range: antenna radiation pattern, radar cross section and absorber reflectivity measurements”. *Helsinki University* (2006).

[7] D. Paris, W. Leach and E. Joy. “Basic theory of probe-compensated near-field measurements”. *IEEE Trans. Antennas Propag.* 26, 373-379 (1978).

[8] P. Fuerholz and A. Murk. “Phase-corrected near-field measurements of the TELIS telescope at 637”. *IEEE Trans. Antennas Propag.* 57, 2518-2525 (2009).

[9] Z. Lou, J. Hu, K. M. Zhou, et al. “A quasi-optical vector near-field measurement system at terahertz band”. *Rev. Sci. Instrum,* 85, 064702 (2014).

[10] J. Hu, Z. Lou, Q. J. Yao, et al. “THz vector field measurement comparison between on-the-fly and step scan method”. *IEEE Trans. THz Sci. Technol,* 7, 27-35 (2017).

[11] S. Li. “Development of atmospheric observation equipment for terahertz band and investigation of the atmospheric transmission measurements”. *University of Chinese Academy of Science* (2016).

[12] A. Newell. “Error analysis techniques for planar near-field measurements”. *IEEE Trans. Antenna Propag.* 36, 754-768 (1988).

[13] X. L. Zhang, Z. Lou, J. Hu et al. “A novel wavefront based algorithm for numerical simulation of quasi-optical systems”. *Proc. SPIE*, 1003011 (2016).